Interconversion between Polymeric Orange and Monomeric Green Forms of a Schiff Base-Oxovanadium(IV) Complex

Kiyohiko Nakajima,* Masaaki Kojima,*,† Shunryo Azuma,† Ryuichi Kasahara,††
Masanobu Tsuchimoto,†† Yoshihiro Kubozono,† Hironobu Maeda,† Setsuo Kashino,† Shigeru Ohba,††
Yuzo Yoshikawa,††† and Junnosuke Fujita††††

Department of Chemistry, Aichi University of Education, Igaya, Kariya 448

†Department of Chemistry, Faculty of Science, Okayama University, Tsushima, Okayama 700

††Department of Chemistry, Faculty of Science and Technology, Keio University, Hiyoshi 3-14-1, Kohoku-ku, Yokohama 223

†††Coordination Chemistry Laboratories, Institute for Molecular Science, Myodaiji, Okazaki 444

††††Division of Natural Sciences, International Christian University, Osawa, Mitaka 181

(Received May 17, 1996)

The orange and green forms of the Schiff base-oxovanadium(IV) complex, [VO{sal-(*RR*)-stien}]·MeOH (**1**, green), [VO{sal-(*RR*)-stien}]·2$CHCl_3$ (**2**, green), and [VO{sal-(*RR*)-stien}]·CH_3CN (**3**, orange) (H_2{sal-(*RR*)-stien} = *N*,*N*′-disalicylidene-(*RR*)-1,2-diphenyl-1,2-ethanediamine), have been prepared, and their crystal structures were determined by an X-ray method. The green forms, **1** and **2**, contain mononuclear square pyramidal molecules of the complex, while the orange form **3** consists of individual complexes stacked to give an infinite linear ···V=O···V=O··· chain. **1**, which crystallizes as monoclinic in space group $P2_1$ with Z=4, has the cell parameters a=16.684(2), b=16.923(4), c=9.249(3) Å, β = 105.76(2)°, and V=2513(1) Å^3. **2**, which crystallizes as triclinic in space group $P\bar{1}$ with Z=2, has the cell parameters a = 13.187(3), b = 13.469(3), c = 10.450(3) Å, α = 103.72(2), β = 103.20(3), γ = 63.03(2)°, and V = 1591.2(7) Å^3. **3** crystallizes as triclinic in space group $P\bar{1}$ with Z=2. The cell parameters are a = 13.300(3), b = 13.667(4), c = 7.551(1) Å, α = 90.44(2), β = 94.51(2), γ = 97.36(2)°, and V = 1357(1) Å^3. The final R indices are R = 0.059 and R_W = 0.062 for **1**, R = 0.098 and R_W = 0.090 for **2**, and R = 0.053 and R_W = 0.042 for **3**. The structural characteristics of these complexes are compared and discussed. **3** shows piezochromism (mechanochromism); its color changes from orange to green upon grinding. **1** and **2** turn orange when heated at 120 °C for a few minutes. The extent of conversion either by grinding or heating was studied by EXAFS (X-ray absorption fine structure) and IR spectroscopy. The orange crystals turn green when exposed to chloroform vapor, and the green crystals turn orange upon exposure to acetonitrile vapor.

Numerous Schiff base-oxovanadium(IV) complexes have been prepared and extensively studied. We have reported on the catalytic properties of optically active Schiff base-oxovanadium(IV) complexes on the asymmetric oxidation of sulfides into sulfoxides.[1,2] Most of these oxovanadium(IV) complexes are blue or green, and have a monomeric five-coordinate square pyramidal structure. However, several orange or red oxovanadium(IV) complexes have been reported, in which an infinite chain of ···V=O···V=O··· bonds exists. The first crystallographic study of the polymeric linear chain structure was reported for [VO(salpn)] (H_2salpn = *N*,*N*′-disalicylidene-1,3-propanediamine) by Mathew et al.[3] Although, several orange complexes assigned to have a linear chain structure have been reported so far, only a few crystal structures have been determined by the X-ray method.[4,5] During the course of our recent studies on the isomerization reaction of the diastereomeric pair of an unsymmetrical Schiff base-oxovanadium(IV) complex in a solid and in solution, we could prepare both orange and green crystals for [VO{3-Xsal,sal-(*RR*)-chxn}] (X = MeO, EtO; H_2{3-Xsal,sal-(*RR*)-chxn} = *N*-salicylidene-*N*′-3-substitutedsalicylidene-(*RR*)-1,2-cyclohexanediamine), and found that the orange crystals isomerized much faster by heating than do the green ones in the solid state.[6] A rearrangement of the V^{IV}=O bond seems to occur during the isomerization reaction, though it is known that the V^{IV}=O bond is rather stable and inert. The different V=O bonding properties between the orange and green crystals would be responsible for the different reactivities. We therefore paid attention to the crystal structures of the orange and green forms of these and related complexes. Pasini et al.[7] have discussed the spectroscopic data of several green and orange Schiff base-oxovanadium(IV) complexes. However, there has been no report on the crystal structures of both the orange and green forms of a single complex; this lack of structural information has prevented us from understanding their different properties in the

solid state. In this paper, we report on the crystal structures of both the orange and green forms of [VO{sal-(*RR*)-stien}], piezochromism (mechanochromism) of the orange form, and thermochromism of the green form. The extent of conversion by either grinding or heating was studied by EXAFS and IR spectroscopy. A part of this study has already been briefly reported.[8)]

Experimental

Preparation of Compounds. (*R,R*)-1,2-Diphenyl-1,2-ethanediamine was prepared and resolved by published methods.[9)] The Schiff base, H_2{sal-(*RR*)-stien} was prepared in situ (EtOH) or by the method of Gullotti et al.[10)] Both the green and orange complexes of [VO{sal-(*RR*)-stien}] were prepared according to a previously reported procedure.[8)] Green prismatic crystals of [VO{sal-(*RR*)-stien}]·MeOH (**1**) and [VO{sal-(*RR*)-stien}]·2$CHCl_3$ (**2**) suitable for X-ray diffraction measurements were obtained by recrystallization from CH_2Cl_2–MeOH (1 : 1 v/v) and $CHCl_3$, respectively. Orange prismatic crystals of [VO{sal-(*RR*)-stien}]·CH_3CN (**3**) were obtained by slow evaporation of an acetonitrile solution at room temperature.

X-Ray Structure Determination. Each crystal was sealed in a capillary tube together with the mother liquor. X-ray diffraction data were collected with a Rigaku AFC-5R (for **1** and **3**) or AFC-5 (for **2**) diffractometer (graphite monochromatized, λ(Mo $K\alpha$) = 0.71073 Å) in the ω–2θ mode. The unit-cell dimensions and their standard deviations were based on 25 centered reflections with 2θ values between 28 and 30° (**1**, **2**, and **3**). The intensities of three standard reflections were monitored every 150 reflections, and showed no detectable changes during data collections. The absorption corrections were applied for **2** by a numerical-integration method and **3** based on ψ-scan data. The structures were solved by direct methods. All non-hydrogen atoms were treated anisotropically, and hydrogen atoms were introduced at calculated positions for **1** with isotropic temperature factors of their parent carbon atoms. Vanadium and chlorine atoms were refined anisotropically and the other non-hydrogen atoms isotropically for **2**. For **3**, the non-hydrogen atoms were treated anisotropically, except those of the acetonitrile molecules. The positions of the hydrogen atoms were fixed and the isotropic temperature factors were fixed to be equal to those of the non-hydrogen atoms to which the H atoms are attached. The calculations were performed using SHELXS-86[11)] and Xtal3.2[12)] for **1**, CRYSTAN-GM[13)] for **2** and TEXSAN[14)] for **3**. The crystallographic data and experimental details are listed in Table 1, and the atomic parameters of the non-hydrogen atoms are given in Tables 2, 3, and 4.

Tables of the anisotropic thermal parameters, coordinates of the hydrogen atoms, all bond lengths and angles, and the complete $F_o - F_c$ data are deposited as Document No. 69068 at the Office of the Editor of Bull. Chem. Soc. Jpn.

X-Ray Absorption Measurements. V K-edge extended X-ray absorption fine structure (EXAFS) spectra were measured in the fluorescence mode at room temperature at the BL-7C of Photon Factory of the National Laboratory of High Energy Physics (KEK-PF, Tsukuba), with a Si (111) sigital focusing monochromator under the ring conditions of a position energy of 2.5 GeV and a ring current of 350—200 mA. EXAFS data analyses were performed with the programs "XAFS93" and "MBF93" developed by one of the authors (H. M.).

Other Measurements. IR spectra were recorded on a JASCO 810 spectrophotometer as Nujol mulls. UV-vis and reflection spectra were obtained on a Hitachi U-3400 spectrophotometer. X-ray powder diffraction (XRD) patterns of orange and green samples were recorded on a Rigaku RAD 1C diffractometer with monochromatized Cu $K\alpha$ radiation. A thermal analysis was carried out using a ULVAC TA-1500 thermal analyzer.

Results and Discussion

The IR spectra of **1** and **2** in Nujol mull showed V=O stretching at 990 cm^{-1}, while that of **3** at 860 cm^{-1}. From these values, **1** and **2** are suggested to have a monomeric structure, and **3** a polymeric linear chain structure.[3,6,7)]

The crystal structures of these complexes were determined by an X-ray method. The numbering system of the atoms for **2** is the same as that for **1**, except for the solvent of crystallization. Selected bond distances and bond angles of **1** are listed in Table 5. **1** contains two independent complexes, **A** and **B**, in the crystal. Figure 1 shows perspective views of these two complexes. The geometry around each vanadium atom is a distorted square pyramid and the tetradentate Schiff base ligand occupies the basal sites. The vanadium atom in each complex is displaced by 0.595(2) Å (**A**) or 0.569(2) Å (**B**) toward the apical oxo ligand from the least-squares basal plane defined by O(n1), O(n2), N(n1), and N(n2) (n = 1,2), respectively. **A** and **B** differ from one another with respect to the orientation of the (*RR*)-stien phenyl groups.

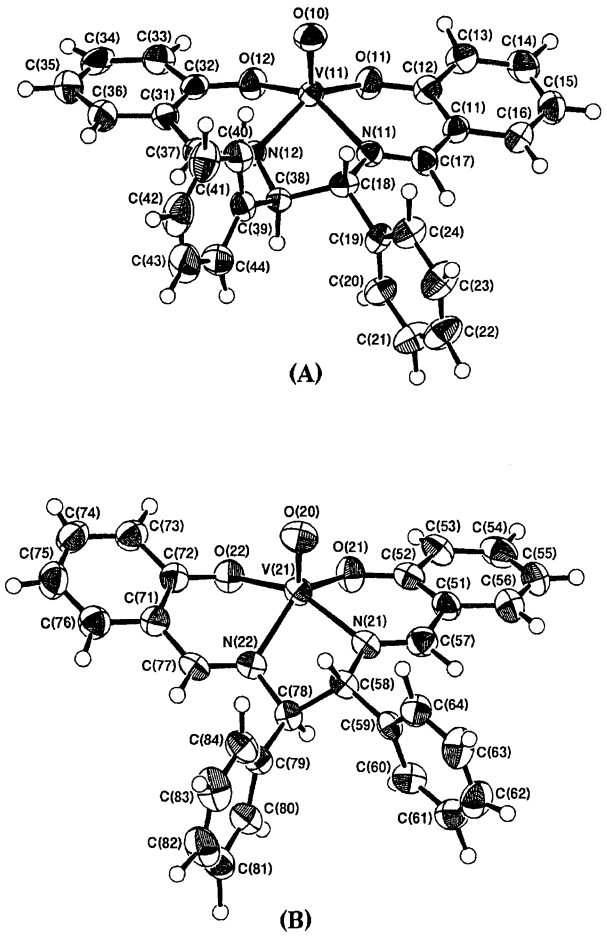

Fig. 1. ORTEP drawing of **1**.

Table 1. Crystallographic Data

Complex	[VO{sal-(*RR*)-stien}]·CH_3OH **1**	[VO{sal-(*RR*)-stien}]·$2CHCl_3$ **2**	[VO{sal-(*RR*)-stien}]·CH_3CN **3**
Formula	$C_{29}H_{26}N_2O_4V$	$C_{30}H_{24}N_2Cl_6O_3V$	$C_{30}H_{25}N_3O_3V$
FW	517.48	724.19	526.49
Crystal system	Monoclinic	Triclinic	Triclinic
Space group	$P2_1$	$P\bar{1}$	$P\bar{1}$
a/Å	16.684(2)	13.187(3)	13.300(3)
b/Å	16.923(4)	13.469(3)	13.667(4)
c/Å	9.249(3)	10.450(3)	7.551(1)
α/°		103.72(2)	90.44(2)
β/°	105.76(2)	103.20(3)	94.51(2)
γ/°		63.03(2)	97.36(2)
Z	4	2	2
V/Å^3	2513(1)	1591.2(7)	1357(1)
μ(Mo$K\alpha$) / cm^{-1}	4.17	3.25	3.86
Crystal color	Green	Green	Orange
Crystal habit	Prismatic	Prismatic	Prismatic
Crystal size / mm^3	0.4×0.4×0.3	0.3×0.4×0.7	0.2×0.3×0.5
D_{calcd}/ gcm^{-3}	1.37	1.51	1.29
Scan type	ω–2θ	ω–2θ	ω–2θ
Scan speed /° min^{-1}	8	6	8
$2\theta_{max}$/°	60	50	60
Reflections measd	$\pm h$, $+k$, $+l$	$+h$, $\pm k$, $\pm l$	$+h$, $\pm k$, $\pm l$
No. of reflections measd	8003	5870	7063
No. of reflections obsd [$\|F_o\| > 3\sigma(\|F_o\|)$]	5038	3879	3563
R[a)]	0.059	0.098	0.053
R_W[b)]	0.062	0.090	0.042

a) $R = \sum\||F_o| - |F_c|\|/\sum|F_o|$, b) $R_W = [\sum w(|F_o| - |F_c|)^2/\sum w|F_o|^2]^{1/2}$.

The five-membered central chelate ring in each complex takes a λ-*gauche* conformation and the phenyl groups are in the equatorial positions; however, the chelate ring of **B** (torsion angle; N(21)–C(58)–C(78)–N(22) 55.7(7)°) is more severely distorted than that of **A** (torsion angle; N(11)–C(18)–C(38)–N(12) 34.6(7)°). The V(11)–O(10) bond length, 1.593(6) Å, in **A** is similar to V(21)–O(20), 1.606(6) Å in **B** and these bond lengths are within the range of a typical V=O distance (1.57—1.62 Å).[3] Figure 2 shows the packing diagram of the unit cell of **1**. There are four monomeric complexes and four methanol molecules in a unit cell. **A** and **B** face each other, disposing the V=O groups in the opposite directions. The nearest distance between V(11) (**A**) and V(21) (**B**) is 4.814(1) Å, and no interaction between the two vanadium atoms is suggested.

2 also contains two independent complexes, **C** and **D**, in the crystal. The structures of **C** and **D** are similar to those of **A** and **B** in **1**, respectively. Selected bond distances and bond angles of **2** are listed in Table 6. The vanadium atom in each complex is displaced by 0.594 Å (**C**) or 0.579 Å (**D**) toward the apical oxo ligand from the least-squares basal plane. Figure 3 shows the packing diagram of the unit cell of **2**. **C** and **D** face each other, disposing the V=O groups in the opposite directions. The nearest distance between V(11) (**C**) and V(21) (**D**) is 6.297(3) Å, and no interaction is suggested.

Figure 4 shows the structure of **3**, and Fig. 5 the packing diagram of the unit cell. Selected bond distances and

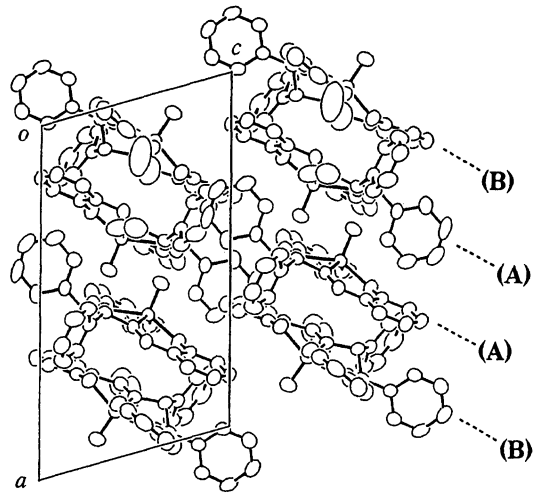

Fig. 2. Projection of the structure of **1** as viewed down the *b*-axis.

bond angles are listed in Table 7. An oxo ligand bridges two vanadium atoms, and a linear chain structure with ···V=O···V=O··· bonds is constructed. The geometry around the vanadium atom is a distorted octahedron. The two metal complex subunits in the unit cell, **E** and **F**, differ by a 180° rotation but otherwise have the identical structural parameters. The V=O bond lengths [V(1A)–O(1A); 1.625(5) Å,V(1B)–O(1B); 1.636(5) Å] are larger than those of **1** and **2** since the oxo ligand coordinates at the position trans to the oxo ligand of

Table 2. Atomic Coordinates ($\times 10^4$) and U_{eq} Values for **1**

Atom	x	y	z	U_{eq}[a)]($Å^2 \times 10^3$)	Atom	x	y	z	U_{eq}[a)]($Å^2 \times 10^3$)
V(11)	6189.6(5)	3702.5	5725(1)	35.2(3)	C(37)	5419(4)	4519(4)	2837(6)	44(2)
V(21)	8666.2(5)	3516.9(6)	4023(1)	39.1(3)	C(38)	5617(3)	3135(3)	2470(6)	35(2)
O(3)	3638(4)	3979(4)	5004(7)	115(3)	C(39)	4759(4)	3093(3)	1314(6)	42(2)
O(4)	7896(4)	8720(6)	14320(8)	163(4)	C(40)	4032(4)	3045(4)	1807(7)	54(2)
O(10)	5395(2)	3595(3)	6366(4)	53(2)	C(41)	3254(4)	3019(4)	781(8)	65(3)
O(11)	7201(2)	3559(2)	7291(4)	48(1)	C(42)	3186(4)	3016(5)	−723(8)	75(3)
O(12)	6489(2)	4802(2)	5813(4)	45(1)	C(43)	3887(5)	3053(5)	−1218(7)	77(3)
O(20)	9306(2)	3699(3)	3060(5)	57(2)	C(44)	4687(4)	3080(4)	−193(7)	58(3)
O(21)	8482(2)	2402(2)	4176(5)	49(2)	C(51)	9645(4)	2027(3)	6233(7)	45(2)
O(22)	7575(2)	3633(2)	2632(4)	50(1)	C(52)	8965(4)	1863(4)	5002(7)	44(2)
N(11)	6413(3)	2600(3)	4926(5)	36(2)	C(53)	8750(4)	1052(3)	4675(7)	51(2)
N(12)	5696(3)	3854(3)	3470(5)	35(1)	C(54)	9223(4)	461(4)	5538(8)	62(3)
N(21)	9484(2)	3444(3)	6143(5)	37(1)	C(55)	9926(4)	632(4)	6698(8)	61(3)
N(22)	8403(3)	4548(3)	5035(5)	40(2)	C(56)	10114(4)	1409(4)	7065(7)	60(3)
C(1)	3481(5)	4725(5)	4160(10)	89(4)	C(57)	9837(4)	2820(4)	6792(7)	46(2)
C(2)	8300(9)	7979(9)	14890(10)	195(8)	C(58)	9691(3)	4243(3)	6823(6)	38(2)
C(11)	7500(3)	2178(3)	7090(6)	38(2)	C(59)	10274(3)	4260(3)	8395(6)	36(2)
C(12)	7592(3)	2901(4)	7893(6)	42(2)	C(60)	10022(4)	4070(4)	9663(7)	48(2)
C(13)	8120(3)	2922(4)	9362(6)	48(2)	C(61)	10564(4)	4077(4)	11045(7)	52(2)
C(14)	8560(4)	2261(4)	9990(7)	57(3)	C(62)	11385(4)	4275(4)	11234(7)	61(3)
C(15)	8510(4)	1558(4)	9192(7)	53(2)	C(63)	11647(4)	4458(4)	10002(8)	57(3)
C(16)	7988(4)	1515(4)	7778(7)	50(2)	C(64)	11105(4)	4432(4)	8585(7)	49(2)
C(17)	6945(4)	2075(3)	5611(6)	42(2)	C(71)	7457(4)	5050(4)	2751(7)	47(2)
C(18)	5777(3)	2394(3)	3461(6)	38(2)	C(72)	7307(3)	4316(4)	1979(7)	43(2)
C(19)	5993(3)	1679(3)	2643(6)	39(2)	C(73)	6811(4)	4316(4)	461(7)	51(2)
C(20)	6641(4)	1715(4)	1956(7)	47(2)	C(74)	6504(4)	5017(4)	−229(7)	56(2)
C(21)	6813(4)	1045(4)	1211(8)	62(3)	C(75)	6639(4)	5740(4)	534(8)	60(3)
C(22)	6368(4)	362(4)	1173(8)	63(3)	C(76)	7119(4)	5743(4)	2026(7)	52(2)
C(23)	5716(4)	349(4)	1848(8)	61(3)	C(77)	7941(3)	5098(3)	4307(7)	43(2)
C(24)	5533(4)	992(4)	2583(7)	49(2)	C(78)	8828(3)	4630(3)	6643(6)	37(2)
C(31)	5523(4)	5267(3)	3558(6)	41(2)	C(79)	8869(3)	5449(3)	7285(6)	39(2)
C(32)	6093(3)	5384(3)	4981(6)	40(2)	C(80)	8386(4)	5621(4)	8268(7)	53(2)
C(33)	6247(4)	6173(4)	5488(7)	51(2)	C(81)	8403(4)	6358(4)	8913(7)	63(3)
C(34)	5827(4)	6789(3)	4656(7)	55(3)	C(82)	8898(4)	6944(4)	8563(9)	71(3)
C(35)	5251(5)	6672(4)	3309(8)	64(3)	C(83)	9369(4)	6794(4)	7572(9)	69(3)
C(36)	5105(4)	5918(4)	2746(7)	56(3)	C(84)	9350(4)	6044(4)	6956(7)	53(2)

a) $U_{eq} = 1/3\{\sum_i \sum_j U_{ij} a_i^* a_j^* \boldsymbol{a}_i \cdot \boldsymbol{a}_j\}$.

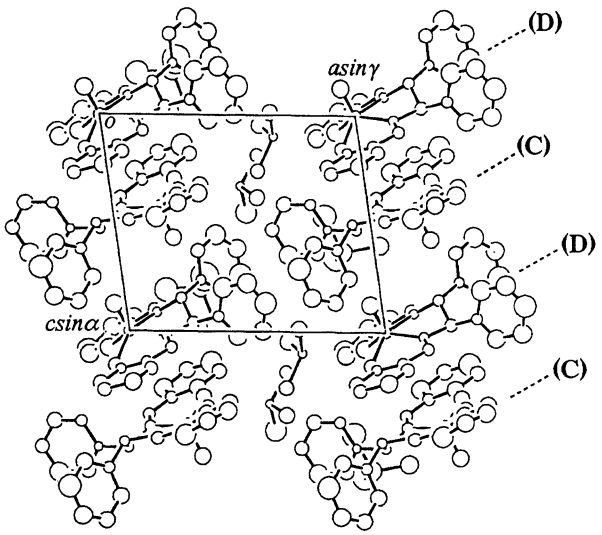

Fig. 3. Projection of the structure of **2** as viewed down the *b*-axis.

the neighboring complex. The V=O bond distance reported for the polymeric [VO(salpn)] complex (1.633(9) Å)[3] is very close to our result. The longer V–O distance is consistent with the lower stretching frequency (vide ante). The bond lengths of V(1A)–O(1B) and V(1B)–O(1A′) [2.188(5) Å and 2.196(5) Å] are slightly smaller than the corresponding bond length of [VO(salpn)] (2.213(9) Å).[3] The vanadium atom of **3** is displaced by only 0.300(4) Å for **E** and 0.306(4) Å for **F** from each basal plane, which is due to the interaction of the oxo ligand with the neighboring vanadium atom to form a distorted octahedral structure.

Most oxovanadium(IV) complexes containing tetradentate Schiff base ligands derived from 1,2-diamines take the monomeric green forms. On the other hand, it is reported that the oxovanadium(IV) complexes with tetradentate Schiff base ligands derived from 1,3-diamines are orange and have a polymeric structure in the solid state, and green forms have not been obtained.[15] We could obtain both the orange and green forms of [VO{sal-(*RR*)-stien}]. Figure 6 shows the

Table 3. Atomic Coordinates ($\times 10^3$) and B_{eq} Values for **2**

Atom	x	y	z	B_{eq}[a)](Å^2)	Atom	x	y	z	B_{eq}[a)](Å^2)
V(11)	158.6(3)	−178.2(2)	−567.4(3)	4.6	C(31)	406(2)	−159(2)	−547(2)	4.8
V(21)	0	0	0	3.4	C(32)	393(2)	−258(2)	−628(2)	4.5
Cl(1A)	−402.0(9)	173.4(9)	−532(1)	13.8	C(33)	493(2)	−355(2)	−674(2)	4.9
Cl(1B)	−502(1)	151(1)	−339(1)	15.2	C(34)	598(2)	−344(2)	−637(2)	5.3
Cl(1C)	−277.1(9)	−22.9(8)	−398.0(9)	10.7	C(35)	607(2)	−258(2)	−590(2)	5.1
Cl(2A)	−577.0(9)	−166(1)	−190(1)	13.9	C(36)	516(2)	−165(2)	−526(2)	6.2
Cl(2B)	−358(1)	−326(1)	−251(1)	17.1	C(37)	309(2)	−57(1)	−511(2)	3.8
Cl(2C)	−447.1(8)	−341.0(8)	−32.7(9)	9.7	C(38)	116(1)	70(1)	−495(1)	3.0
Cl(3A)	−590.1(7)	−572.4(8)	−618.5(9)	9.4	C(39)	153(1)	142(1)	−376(2)	3.3
Cl(3B)	−773.2(8)	−592.8(6)	−815.9(7)	7.8	C(40)	182(2)	111(2)	−245(2)	4.7
Cl(3C)	−810.5(9)	−522(1)	−547.9(8)	12.5	C(41)	232(2)	177(2)	−134(2)	4.8
Cl(4A)	−246.2(8)	−621.8(9)	44.8(8)	10.4	C(42)	241(2)	264(2)	−155(2)	5.4
Cl(4B)	−77.5(8)	−589.5(7)	258.1(7)	8.2	C(43)	204(2)	299(2)	−289(3)	6.8
Cl(4C)	−29.4(8)	−668.1(8)	−13.1(8)	9.6	C(44)	158(2)	232(2)	−401(2)	5.0
O(10)	180(1)	−222(1)	−430(1)	5.0	C(51)	−251(2)	−10(2)	−29(2)	3.8
O(11)	87(1)	−257(1)	−704(1)	4.6	C(52)	−239(2)	75(2)	43(2)	3.2
O(12)	293(1)	−265(1)	−650(1)	4.8	C(53)	−335(2)	162(2)	106(2)	5.4
O(20)	7(1)	43(1)	−124(1)	5.3	C(54)	−443(2)	166(2)	88(2)	6.4
O(21)	−141(1)	86(1)	77(1)	4.5	C(55)	−459(2)	63(2)	−18(2)	5.3
O(22)	72(1)	71(1)	156(1)	4.1	C(56)	−364(2)	−25(2)	−64(2)	5.1
N(11)	−2(1)	−35(1)	−565(1)	3.4	C(57)	−162(2)	−111(1)	−99(2)	4.0
N(12)	211(1)	−48(1)	−522(1)	3.6	C(58)	34(1)	−222(1)	−152(1)	3.3
N(21)	−58(1)	−118(1)	−87(1)	2.7	C(59)	−8(1)	−309(1)	−235(2)	3.0
N(22)	144(1)	−144(1)	20(1)	3.0	C(60)	−15(2)	−391(2)	−180(2)	5.0
C(1)	−361(3)	124(4)	−366(4)	12	C(61)	−56(2)	−467(2)	−259(3)	6.8
C(2)	−490(4)	−306(4)	−204(4)	12	C(62)	−84(2)	−466(2)	−381(2)	5.3
C(3)	−746(2)	−513(2)	−671(1)	5.2	C(63)	−76(2)	−390(2)	−444(2)	5.9
C(4)	−110(2)	−669(2)	99(2)	5.1	C(64)	−40(2)	−312(2)	−370(2)	4.1
C(11)	−119(2)	−130(2)	−698(2)	3.6	C(71)	264(2)	−52(2)	142(2)	3.3
C(12)	−22(2)	−238(2)	−745(2)	4.9	C(72)	184(2)	52(2)	173(2)	3.0
C(13)	−47(2)	−330(2)	−820(2)	4.4	C(73)	217(2)	136(2)	239(2)	4.3
C(14)	−165(2)	−305(2)	−860(2)	6.5	C(74)	326(2)	125(2)	270(2)	4.0
C(15)	−254(2)	−205(2)	−825(2)	4.8	C(75)	419(2)	12(2)	233(2)	5.1
C(16)	−234(2)	−106(2)	−742(2)	5.6	C(76)	384(2)	−66(2)	171(2)	4.0
C(17)	−100(1)	−36(1)	−620(2)	3.5	C(77)	247(1)	−157(1)	74(2)	3.5
C(18)	10(1)	58(1)	−468(1)	3.0	C(78)	129(1)	−256(1)	−38(2)	3.7
C(19)	−93(1)	170(1)	−469(2)	2.5	C(79)	240(1)	−360(1)	−69(2)	3.4
C(20)	−144(2)	222(1)	−587(2)	3.4	C(80)	300(2)	−424(2)	22(2)	5.4
C(21)	−235(2)	324(2)	−587(2)	4.6	C(81)	400(2)	−526(2)	−4(2)	5.6
C(22)	−282(2)	385(2)	469(2)	4.1	C(82)	428(2)	−551(2)	−130(2)	6.6
C(23)	−232(2)	334(2)	−353(2)	5.7	C(83)	375(2)	−488(2)	−222(2)	5.8
C(24)	−134(2)	221(2)	−360(2)	4.1	C(84)	278(2)	−392(2)	−200(2)	5.9

a) $B_{eq} = 4/3\{\sum_i \sum_j B_{ij} \boldsymbol{a}_i \cdot \boldsymbol{a}_j\}$.

reflection spectra of the complexes. A broad band at 590 nm of the green complexes (**1** and **2**) corresponds to the d–d absorption band in dichloromethane (592 nm). The reflection band of **3** appeared at 883 nm. When **3** is dissolved in dichloromethane, the color of the solution turns green and the absorption spectrum is identical to those of **1** and **2**. Thus, it is concluded that the polymeric structure of **3** changes to a monomeric one in solution.

3 shows piezochromism (mechanochromism); it exhibits a color change from orange to green upon grinding. The green powder obtained upon grinding showed the V=O stretching band at 990 cm^{-1} in addition to the original 860 cm^{-1} absorption in the IR spectrum, suggesting the formation of a monomeric species. The intensity ratio between the two V=O stretching bands (990 and 860 cm^{-1}) indicates the proportion of disassembling, and depends on the extent of grinding. We measured the IR spectrum of the sample, **a**, obtained by thoroughly grinding **3** in a mortar, and found that about 90% of **3** had been converted to the green form.

We presumed that either pressure or heat would cause the color change and studied the stability of the orange and green crystals toward pressure and heat. All of complexes **1**, **2**, and **3** were very resistant to pressure; although the complexes were pressed at 10^4 kg cm^{-2} for a few minutes, their color did not change. The color (orange) of **3** remained unchanged even after heating at 150 °C for 2 h. On the other hand, **1** and **2** (green forms) show thermochromism; they turned orange when heated at 120 °C for a few minutes. The orange form

Table 4. Atomic Coordinates ($\times 10^3$) and B_{eq} Values for **3**

Atom	x	y	z	B_{eq}[a)]($Å^2$)	Atom	x	y	z	B_{eq}[a)]($Å^2$)
V(1A)	840.7	885.5	711.5	2.8	C(12B)	500.9(8)	766.2(9)	45(2)	6.3
V(1B)	851.0(1)	863.7(1)	212.7(3)	2.8	C(13A)	1088.4(8)	958.7(7)	688(1)	4.5
O(1A)	829.0(5)	866.7(5)	921.6(6)	2.9	C(13B)	601.8(7)	794.2(7)	103(1)	4.0
O(1B)	864.1(4)	882.4(5)	428.0(7)	2.8	C(14A)	1056.1(8)	852.1(8)	699(1)	4.2
O(2A)	719.0(5)	944.0(5)	637.0(8)	3.7	C(14B)	631.0(8)	898.2(8)	129(1)	4.5
O(2B)	973.1(5)	806.2(5)	171.2(8)	3.7	C(15A)	841.6(6)	673.9(6)	603(1)	3.4
O(3A)	926.6(5)	1012.2(5)	712(1)	3.6	C(15B)	850.7(6)	1074.0(6)	112(1)	3.4
O(3B)	764.0(5)	736.6(5)	186.6(9)	3.7	C(16A)	798.1(7)	568.1(7)	633(1)	4.0
N(1A)	771.2(5)	747.7(5)	629.9(9)	2.9	C(16B)	895.5(8)	1181.5(8)	152(1)	4.0
N(1B)	920.9(5)	1001.3(5)	153.6(8)	2.9	C(17A)	765(1)	538.9(8)	797(2)	5.6
N(2A)	965.9(6)	813.5(6)	711(1)	2.7	C(17B)	900.8(9)	1249.7(9)	18(2)	6.3
N(2B)	724.8(7)	937.9(6)	175(1)	3.3	C(18A)	726(1)	439(1)	818(2)	7.6
N(1S)	407(2)	326(2)	640(3)	18.5	C(18B)	937(1)	1346(1)	58(3)	9
N(1SB)	291(1)	443(1)	217(2)	15.3	C(19A)	724(1)	371(1)	682(3)	10
C(1A)	626.7(7)	898.3(7)	606(1)	3.6	C(19B)	974(1)	1372(1)	231(3)	10
C(1B)	1065.3(7)	8490.8(8)	166(1)	3.8	C(20A)	759(1)	400(1)	523(2)	9
C(2A)	545.9(8)	955.9(8)	588(1)	4.9	C(20B)	968(1)	1307(1)	364(2)	7.8
C(2B)	1145.0(8)	794.3(8)	162(1)	5.4	C(21A)	793.0(9)	499.4(9)	498(2)	6.3
C(3A)	445.9(8)	913(1)	559(2)	7.0	C(21B)	929(1)	1213.9(9)	323(2)	6.2
C(3B)	1243(1)	832(1)	154(2)	7.1	C(22A)	939.7(8)	704.5(8)	731(1)	3.3
C(4A)	419.9(8)	810(1)	534(2)	8.7	C(22B)	753.5(8)	1044.7(8)	207(1)	3.3
C(4B)	1266.5(9)	932(1)	146(2)	9.0	C(23A)	1022.9(8)	640.7(8)	692(1)	4.2
C(5A)	496.4(8)	752.5(9)	546(2)	6.6	C(23B)	669.3(8)	1107.9(8)	154(1)	4.1
C(5B)	1191(1)	992.0(9)	142(2)	7.0	C(24A)	1061.4(8)	639.5(8)	532(1)	5.1
C(6A)	600.3(7)	793.9(7)	584(1)	3.9	C(24B)	633.8(8)	1115.3(9)	−25(1)	5.7
C(6B)	1089.2(7)	953.5(8)	154(1)	4.1	C(25A)	1137(1)	583(1)	501(2)	7.1
C(7A)	674.0(8)	727.3(7)	586(1)	4.1	C(25B)	556(1)	1173(1)	−70(2)	8.0
C(7B)	1016.4(8)	1021.7(7)	138(1)	4.1	C(26A)	1170(1)	528(1)	637(3)	11
C(8A)	1025.7(7)	1030.3(7)	696(1)	3.4	C(26B)	518(1)	1221(1)	70(3)	10
C(8B)	667.2(8)	720.8(7)	143(1)	3.4	C(27A)	1134(1)	530(1)	802(3)	10
C(9A)	1068.8(9)	1128.7(8)	699(1)	5.0	C(27B)	555(2)	1218(1)	240(3)	11
C(9B)	621.0(8)	620.9(8)	128(1)	4.7	C(28A)	1060.5(9)	587.0(9)	830(2)	6.2
C(10A)	1173(1)	1154.2(8)	686(2)	6.6	C(28B)	630(1)	1159.2(8)	282(2)	6.7
C(10B)	517.6(9)	597.7(9)	73(2)	6.3	C(1S)	440(2)	399(2)	632(3)	17.3
C(11A)	1235(1)	1085(1)	678(2)	8.8	C(1SB)	273(1)	359(2)	179(2)	12.0
C(11B)	459.3(9)	667(1)	29(2)	8.0	C(2S)	486(1)	483(1)	576(2)	11.3
C(12A)	1193.7(8)	987(1)	674(2)	7.5	C(2SB)	226(1)	266(1)	188(2)	12.8

a) $B_{eq} = 4/3\{\sum_i \sum_j B_{ij} \boldsymbol{a}_i \cdot \boldsymbol{a}_j\}$.

Table 5. Selected Bond Lengths (l/Å) and Bond Angles (ϕ/°) of **1**

V(11)–O(10)	1.593(6)	V(21)–O(20)	1.606(6)
V(11)–O(11)	1.925(4)	V(21)–O(21)	1.929(5)
V(11)–O(12)	1.916(5)	V(21)–O(22)	1.935(4)
V(11)–N(11)	2.077(6)	V(21)–N(21)	2.070(5)
V(11)–N(12)	2.045(5)	V(21)–N(22)	2.080(7)
O(10)–V(11)–O(11)	110.4(2)	O(20)–V(21)–O(21)	116.3(3)
O(10)–V(11)–O(12)	109.4(2)	O(20)–V(21)–O(22)	105.2(2)
O(10)–V(11)–N(11)	106.0(3)	O(20)–V(21)–N(21)	99.8(2)
O(10)–V(11)–N(12)	104.7(2)	O(20)–V(21)–N(22)	109.6(3)
O(11)–V(11)–O(12)	85.5(2)	O(21)–V(21)–O(22)	90.3(2)
O(11)–V(11)–N(11)	87.2(2)	O(21)–V(21)–N(21)	87.1(2)
O(11)–V(11)–N(12)	144.6(2)	O(21)–V(21)–N(22)	137.9(3)
O(12)–V(11)–N(11)	144.3(2)	O(22)–V(21)–N(21)	154.0(2)
O(12)–V(11)–N(12)	87.3(2)	O(22)–V(21)–N(22)	87.0(2)
N(11)–V(11)–N(12)	78.8(2)	N(21)–V(21)–N(22)	77.9(2)

remained unchanged when the complex was cooled to a very low temperature (−196 °C). The IR spectrum revealed that

Table 6. Selected Bond Lengths (l/Å) and Bond Angles (ϕ/°) of **2**

V(11)–O(10)	1.60(2)	V(21)–O(20)	1.57(2)
V(11)–O(11)	1.90(2)	V(21)–O(21)	1.93(2)
V(11)–O(12)	1.90(2)	V(21)–O(22)	1.96(1)
V(11)–N(11)	2.12(1)	V(21)–N(21)	2.02(1)
V(11)–N(12)	2.08(2)	V(21)–N(22)	2.02(1)
O(10)–V(11)–O(11)	109.5(8)	O(20)–V(21)–O(21)	115.0(6)
O(10)–V(11)–O(12)	107.6(6)	O(20)–V(21)–O(22)	106.1(8)
O(10)–V(11)–N(11)	104.4(6)	O(20)–V(21)–N(21)	102.1(7)
O(10)–V(11)–N(12)	105.9(7)	O(20)–V(21)–N(22)	106.1(6)
O(11)–V(11)–O(12)	86.4(7)	O(21)–V(21)–O(22)	86.4(6)
O(11)–V(11)–N(11)	88.8(6)	O(21)–V(21)–N(21)	88.6(6)
O(11)–V(11)–N(12)	144.4(7)	O(21)–V(21)–N(22)	138.7(7)
O(12)–V(11)–N(11)	147.4(7)	O(22)–V(21)–N(21)	150.7(6)
O(12)–V(11)–N(12)	86.5(7)	O(22)–V(21)–N(22)	86.8(5)
N(11)–V(11)–N(12)	78.8(6)	N(21)–V(21)–N(22)	78.1(6)

Table 7. Selected Bond Lengths (l/Å) and Bond Angles (ϕ/°) of **3**

V(1A)–O(1A)	1.625(5)	V(1B)–O(1B)	1.636(5)
V(1A)–O(2A)	1.942(6)	V(1B)–O(2B)	1.939(6)
V(1A)–O(3A)	1.948(7)	V(1B)–O(3B)	1.960(7)
V(1A)–N(1A)	2.056(7)	V(1B)–N(1B)	2.056(7)
V(1A)–N(2A)	2.040(8)	V(1B)–N(2B)	2.072(9)
	V(1A)–O(1B)	2.188(5)	
	V(1B)–O(1A′)	2.196(5)	
O(1A)–V(1A)–O(2A)	102.8(3)	O(1B)–V(1B)–O(2B)	101.9(3)
O(1A)–V(1A)–O(3A)	103.0(3)	O(1B)–V(1B)–O(3B)	102.9(3)
O(1A)–V(1A)–O(1B)	169.1(3)	O(1B)–V(1B)–O(1A′)	169.7(3)
O(1A)–V(1A)–N(1A)	94.9(3)	O(1B)–V(1B)–N(1B)	95.0(3)
O(1A)–V(1A)–N(2A)	93.0(3)	O(1B)–V(1B)–N(2B)	94.3(3)
O(2A)–V(1A)–O(3A)	92.5(3)	O(2B)–V(1B)–O(3B)	93.2(3)
O(2A)–V(1A)–O(1B)	84.9(2)	O(2B)–V(1B)–O(1A′)	84.6(2)
O(2A)–V(1A)–N(1A)	91.2(3)	O(2B)–V(1B)–N(1B)	90.7(3)
O(2A)–V(1A)–N(2A)	162.8(3)	O(2B)–V(1B)–N(2B)	162.0(3)
O(3A)–V(1A)–O(1B)	84.1(3)	O(3B)–V(1B)–O(1A′)	84.6(3)
O(3A)–V(1A)–N(1A)	160.4(3)	O(3B)–V(1B)–N(1B)	160.5(3)
O(3A)–V(1A)–N(2A)	90.4(3)	O(3B)–V(1B)–N(2B)	90.6(3)
O(1B)–V(1A)–N(1A)	77.0(2)	O(1A′)–V(1B)–N(1B)	76.8(2)
O(1B)–V(1A)–N(2A)	78.6(3)	O(1A′)–V(1B)–N(2B)	78.3(3)
N(1A)–V(1A)–N(2A)	80.7(3)	N(1B)–V(1B)–N(2B)	80.2(3)
	V(1A)–O(1A)–V(1B′)	165.5(3)	
	V(1A)–O(1B)–V(1B)	164.7(3)	

about 80% of the monomeric form (**2**) converted into the orange form after heating at 100 °C for 10 min. Prolonged heating (100 °C for 110 min, hereafter sample **b**) did not affect the proportion. A thermogravimetric measurement of **2** was carried out; the temperature was raised at the rate of 2 deg min^{-1} up to 150 °C. The loss of two chloroform molecules was observed in the range of ca. 40 to 90 °C. Thus, the color change seems to occur after evaporation of the chloroform molecules.

The extent of conversion by either grinding or heating was also studied by EXAFS. The magnitude and imaginary parts of the Fourier transform ($\Phi(r)$) for **2**, **3**, **a**, and **b** were obtained from EXAFS oscillations ($k^3\chi(k)$) (Fig. 7). Inverse Fourier transforms were performed on the r-region shown in Fig. 7. A non-liner least-squares fitting was applied to the inverse-Fourier transform EXAFS to determine the structural parameters, according to the EXAFS formula within the framework of harmonic approximation.[16] Following an EXAFS workshop reported,[17] a double Fourier-transform was employed in the fitting, by which the theoretical EXAFS function was filtered in the same manner as the observed function in order to eliminate the termination effect in the Fourier transform.

The values of the mean-squares displacement ($\sigma(2)$), the mean free path of photoelectron ($\lambda(k)$), and the shift from the threshold energy estimated from the first inflection point on the absorption edge (ΔE) for **2** and **3** were determined, where three and four shell fittings were adopted, respectively, on the basis of the distances (r) between the V atom and the first neighboring atoms by crystal-structure analyses for **2**

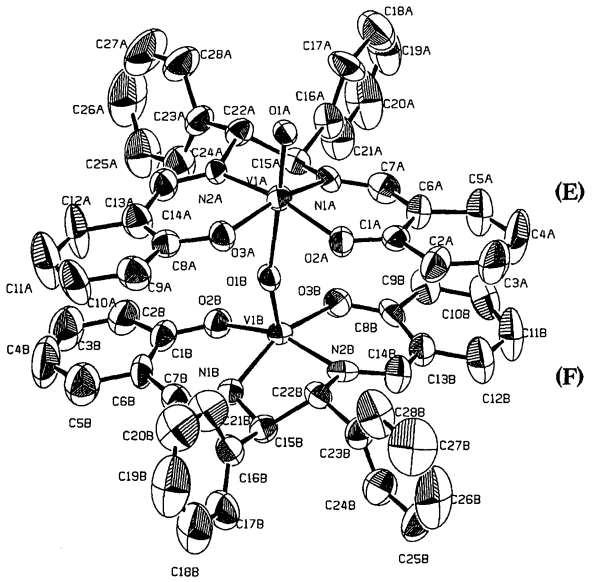

Fig. 4. ORTEP drawing of **3**.

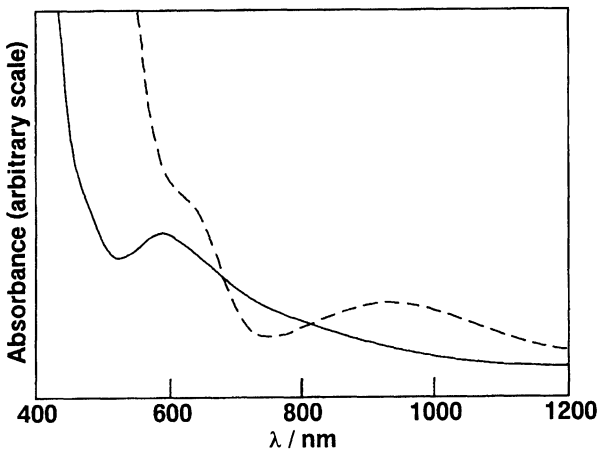

Fig. 6. Reflection spectra of **1**,**2** (—), and **3** (- - -).

and **3**. For **2**, the values of the coordination number (N) and the distance (r) were fixed to 1 and 1.604 Å in the first shell, 2 and 1.916 Å in the second, and 2 and 2.060 Å in the third. For **3**, the values of N and r were fixed to 1 and 1.625 Å in the first shell, 2 and 1.945 Å in the second, 2 and 2.048 Å in the third, and 1 and 2.188 Å in the fourth. The values of $\sigma(2)$, $\lambda(k)$, and ΔE determined in these fittings were 0.018(3) Å^2, 1.00(9)k Å, and −2.9(6) eV in all shells for **2**, and 0.0008(4) Å^2, 1.16(9)k Å, and 2.6(6) eV in the third shell for **3**, and 0.0045(4) Å^2, 1.16(9)k Å, and 2.6(6) eV in the other shells for **3**.

The values of the volume fraction (W_F) of **2** and **3** in samples **a** and **b** were determined by a parameter-fitting to the Fourier-transform EXAFS for **a** and **b**. In these fittings the values of N, r, $\lambda(k)$, and ΔE were fixed to those of **2** and **3**, and the mean values of $\sigma(2)$ for **2** and **3** were used.

Sample **a** contains both monomeric and polymeric forms; the W_F values, 0.67(8), for monomeric form is large than that, 0.33(7), for the polymeric form. Grinding the polymeric form, **3**, induces a conversion from the polymeric to the monomeric form. The results are consistent with those by IR spectroscopy, although the W_F value of the monomeric form is underestimated compared with that determined by the IR method.

Sample **b** also contains both monomeric and polymeric forms. In contrast to **a**, the W_F values (0.64(9)) for the polymeric form is larger than that (0.36(19)) for the monomeric form. The conversion from the monomeric form to the polymeric form by heating **2** has also been confirmed by EXAFS.

Conversions from the polymeric to the monomeric form by grinding the polymeric form, and from the monomeric to the polymeric form by heating the monomeric form have been confirmed by the IR and EXAFS methods.

As described above, the polymeric structure appears to be a more thermodynamically stable form. It is notable that the polymeric linear-chain structure can not be changed to a monomeric one by either heat or pressure, but only by grinding. Grinding presumably cleaves the ···V=O···V=O··· bonds to yield a monomeric species. The green product obtained by grinding reverts to orange when moistened with a small amount of acetonitrile or acetone, or by exposure to acetonitrile vapor. These results suggest a reformation of the

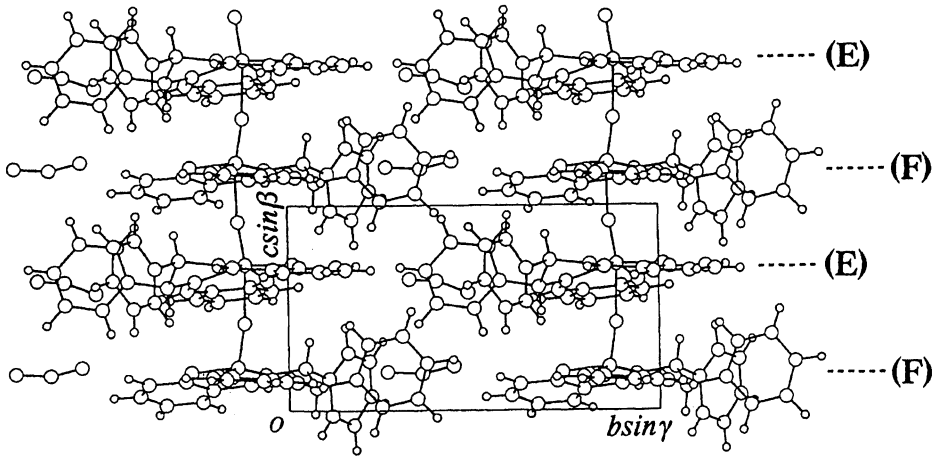

Fig. 5. Projection of the structure of **3** as viewed down the a-axis.

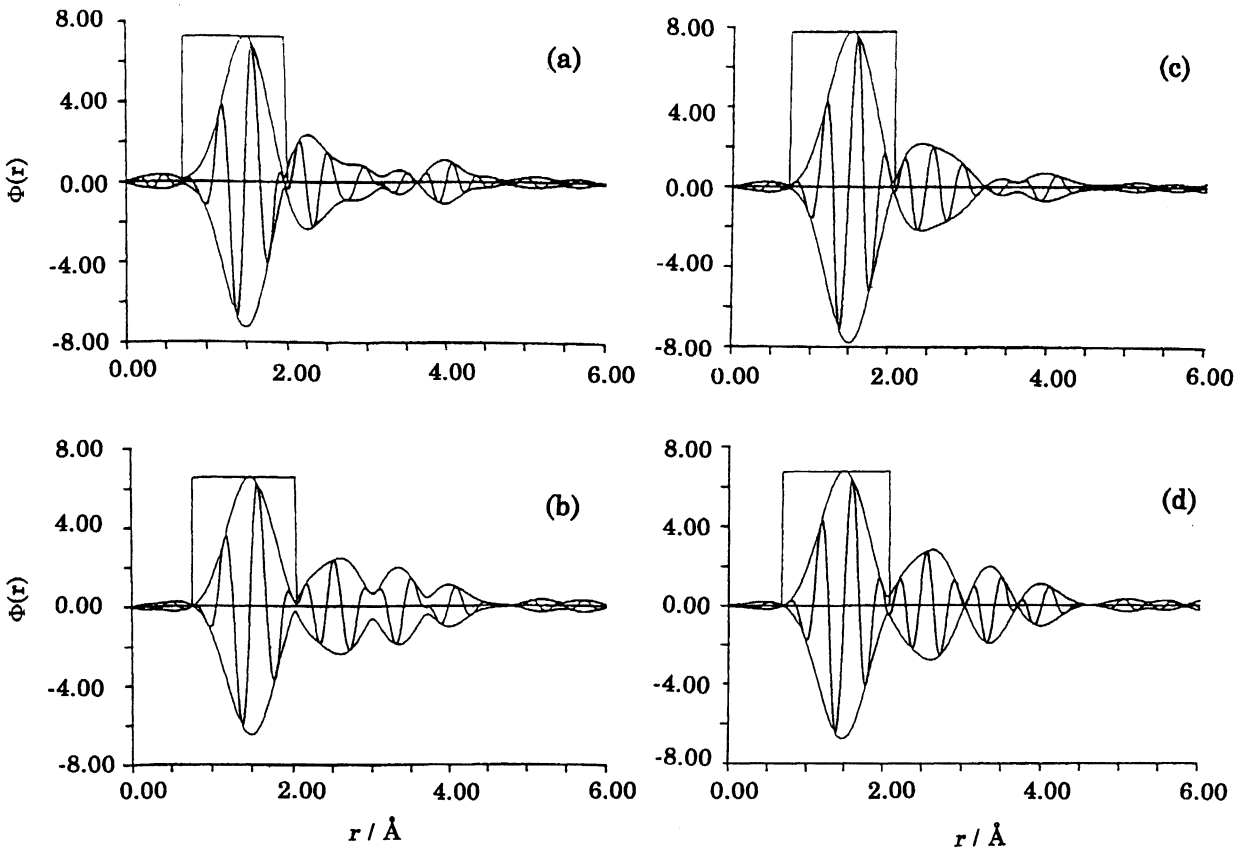

Fig. 7. The magnitude (envelope) and imaginary part of $\Phi(r)$ for (a) complex **2**, (b) complex **3**, (c) sample **a**, and (d) sample **b**.

polymeric linear-chain structure. This color change could be made repeatedly. We also observed that the orange crystals turned green upon exposure to chloroform vapor, and that the green crystals turned orange when exposed to acetonitrile vapor. Accordingly, X-ray powder diffraction measurements of these samples were carried out. The green product obtained by grinding **3** ([VO{sal-(*RR*)-stien}]·CH_3CN) was not crystalline. Probably, the loss of crystallinity was related to the evaporation of the acetonitrile molecule. Figure 8 compares the X-ray powder diffraction patterns of the orange samples. The diffraction patterns of **3** (Fig. 8-(a)) and that of the orange crystals obtained by exposing the green crystals to acetonitrile vapor (Fig. 8-(b)) were almost identical, and we thus conclude that the structures of these two samples are the same. Pasini and Gullotti[7] obtained [VO{sal-(*SS*)-stien}] as a yellow-brown powder, and reported that the compound became green upon grinding. However, their green form was not stable and eventually became brown, and they could not record its reflection spectrum. We also measured the X-ray diffraction patterns of the green complex, [VO{sal-(*RR*)-stien}]·$2CHCl_3$ (**2**) and the green crystals obtained by moistening the orange crystals with a small amount of chloroform. When these crystals are ground, they easily lose chloroform molecules and have a tendency to change to the stable orange form. We found that the diffraction pattern of a sample changes with the passage of time. Thus, the diffraction patterns of the two green samples were not identical, but were similar to each other. We presume that the two samples have

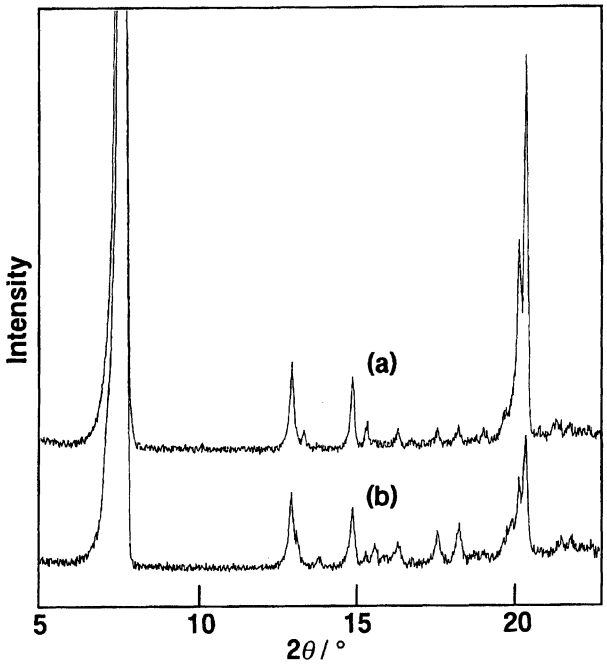

Fig. 8. X-Ray powder diffraction (XRD) patterns of the orange samples; (a): **3**, (b): the orange crystals obtained by exposing the green crystals to acetonitrile vapor.

the same crystal structures.

We have shown that the monomeric green complexes (**1** and **2**) and the polymeric orange complex (**3**) interconvert to

each other in the solid state under appropriate conditions. At first, such an interconversion between the structures of the green and orange complexes seemed to be difficult, since the V=O groups dispose in the opposite directions in the crystals of **1** and **2** (Figs. 2 and 3), while the chain structure (**3**) has a parallel arrangement of V=O groups (Fig. 5) and a substantial rearrangement of molecular orientation is required for interconversion. However, the following two-step mechanism may account for this anomalous behavior. In the first step of the conversion from the orange complex (**3**) to the green one (**1** or **2**), for example, a transfer of the bridging oxygen from one molecule to another in an alternating chain takes place to yield an antiparallel arrangement of the V=O groups. Then, the appropriate molecules translate so that two close molecules face each other, and end up with the structure of the green complex (**1** or **2**). During the course of studies concerning the color change with solvent vapor, we noticed that some crystals changed their color much faster than did others. This observation seems to suggest that the rearrangement starts at the lattice defect sites. Solvent of crystallization may also play an important role in changing the packing structures.

The authors gratefully acknowledge Prof. Koko Maeda of Ochanomizu University, Dr. Kazuo Yamasaki, Professor Emeritus of Nagoya University, and Prof. Peter Luger of Freie Universität Berlin for their fruitful discussions and suggestions. We thank Dr. Hideki Taguchi of Okayama University for the measurement of the X-ray powder diffraction (XRD) patterns and helpful advice about them. The present work was supported by Grants-in-Aid Scientific Research Nos. 05403009, 06640720, and 07640753 from the Ministry of Education, Science and Culture.

References

1) K. Nakajima, M. Kojima, and J. Fujita, *Chem. Lett.*, **1986**, 1483.
2) K. Nakajima, K. Kojima, M. Kojima, and J. Fujita, *Bull. Chem. Soc. Jpn.*, **63**, 2620 (1990).
3) M. Mathew, A. J. Carty, and G. J. Palenik, *J. Am. Chem. Soc.*, **92**, 3197 (1970).
4) A. Serrette, P. J. Carroll, and T. M. Swager, *J. Am. Chem. Soc.*, **114**, 1887 (1992).
5) S. A. Fairhurst, D. L. Hughes, U. Kleinkes, G. J. Leigh, J. R. Sanders, and J. Weisner, *J. Chem. Soc., Dalton Trans.*, **1995**, 321.
6) M. Kojima, K. Nakajima, M. Tsuchimoto, M. Tanaka, T. Suzuta, Y. Yoshikawa, and J. Fujita, *Chem. Lett.*, **1994**, 949.
7) A. Pasini and M. Gullotti, *J. Coord. Chem.*, **3**, 319 (1974).
8) M. Kojima, K. Nakajima, M. Tsuchimoto, P. M. Treichel, S. Kashino, and Y. Yoshikawa, *Proc. Jpn. Acad., Ser. B*, **71**, 175 (1995).
9) E. J. Corey, R. Imwinkelried, S. Pikul, and Y. B. Xiang, *J. Am. Chem. Soc.*, **111**, 5493 (1989); K. Saigo, N. Kubota, S. Takabayashi, and M. Hasegawa, *Bull. Chem. Soc. Jpn.*, **59**, 931 (1986).
10) M. Gullotti, A. Pasini, P. Fantucci, R. Ugo, and R. D. Gillard, *Gazz. Chim. Ital.*, **102**, 855 (1972).
11) G. M. Sheldrick, "SHELXS-86, Program for Crystal Structure Determination," University of Göttingen, Germany (1986).
12) S. R. Hall, H. D. Flack, and J. M. Stewart, "Xtal3.2, Program for X-Ray Crystal Structure Analysis," Universities of Western Australia, Geneva and Maryland (1992).
13) MAC Science, "CRYSTAN-GM, Program for X-Ray Crystal Structure Analysis," MAC Science, Tokyo, Japan (1992).
14) "TEXSAN- TEXRAY Structure Analysis Package," Molecular Structure Corporation (1985).
15) R. L. Farmer and F. L. Urbach, *Inorg. Chem.*, **13**, 587 (1974).
16) T. Ishii, *J. Phys. Condens. Matter*, **4**, 8029 (1992).
17) F. W. Lytle, D. E. Sayers, and E. A. Stern, *Physica B*, **158**, 701 (1989).